Characterization of Piecewise Smooth Images with Wavelets: Application to Noise Variance Estimation

Sylvain Meignen *

LMC-IMAG Laboratory, 51 rue des mathématiques, BP.53,

38041 Grenoble Cedex 9, France

Abstract

We propose a novel approach to the characterization of geometric regions by use of wavelet coefficients. We show that in the absence of noise, geometric regions with edges behave differently from other regions as far as the evolution of their wavelet coefficients through scales is concerned. We use this particularity to identify piecewise smooth subimages in a noisy context on which we perform noise variance estimation, for white noise and $1/f$ noise.

Key words: Noise variance estimation, orthogonal wavelet decomposition, geometric images, textures

* Corresponding author. Tél: +33 4 76 51 43 95, Fax: +33 4 76 63 12 63
Email address: `sylvain.meignen@imag.fr` (Sylvain Meignen).

1 Introduction

The problem of white noise variance estimation has been satisfactory solved by Donoho (Donoho and Johnstone 1994) in the case of piecewise smooth images using orthogonal wavelet decomposition. Natural images very often contain both piecewise smooth and oscillatory subimages which makes the problem of noise variance estimation more complicated. Indeed, most techniques for noise extraction (Donoho and Johnstone 1994) (Rank et al. 1999) are based on the idea that one can roughly isolate the noise from the rest of the image considering a highpass filter. This hypothesis is no longer true with oscillatory images such as textures which have an important high frequency component. In the absence of noise, it is possible to characterize a subset of the piecewise smooth images made by the piecewise smooth images with contour of non-zero length (PSI) through the study of their wavelet coefficients through scales (Mallat 1998). We first show how to retrieve PSI in a noisy context. We then develop new algorithms to estimate the noise variance for white noises and also for $1/f$ noises. They are based on the identification of the image subregions that are PSI on which we perform the noise variance estimation.

We study the behavior of our PSI detector both in the absence and in the presence of noise. In the absence of noise, we test the robustness of the PSI images selection criterion for different block sizes. In the presence of noise, we first show the relevance of the approach we propose to retrieve PSI and then compare our noise variance estimator to a global noise variance estimator defined in (Donoho and Johnstone 1994). We finally illustrate the procedure on artificial and natural images.

2 Multiresolution Framework Presentation

In this paper, we assume that the gray level at each image pixel is the average of a function v over the pixel. In the case of a square image of size N^2, with $N = 2^J$, the gray level at each pixel is:

$$v_k^J = 2^J \int\limits_{C_{J,k}} v(x,y)dxdy = 2^J \int\limits_{\mathbb{R}^2} \Phi(2^J x - k_x)\Phi(2^J y - k_y)v(x,y)dxdy$$
$$=< v, \Phi_{k_x}^J(x)\Phi_{k_y}^J(y) > \qquad (1)$$

where $C_{J,k} = [k_x 2^{-J}, (k_x+1)2^{-J}] \times [k_y 2^{-J}, (k_y+1)2^{-J}]$, $k = (k_x, k_y) \in \{0, 2^J - 1\} \times \{0, 2^J - 1\}$, and Φ is the characteristic function of the interval $[0, 1]$. The definition (1) implies for any $j \leq J$ the inter scales relation:

$$v_k^{j-1} = \frac{1}{2}(v_{2k_x,2k_y}^j + v_{2k_x,2k_y+1}^j + v_{2k_x+1,2k_y}^j + v_{2k_x+1,2k_y+1}^j). \qquad (2)$$

We associate with it the orthogonal complement (detail coefficients):

$$\begin{aligned}
v_{k,1}^{j-1} &= \frac{1}{2}(v_{2k_x,2k_y}^j + v_{2k_x,2k_y+1}^j - v_{2k_x+1,2k_y}^j - v_{2k_x+1,2k_y+1}^j) \\
&= < v, \Phi_{k_x}^{j-1}\Psi_{k_y}^{j-1} > \\
v_{k,2}^{j-1} &= \frac{1}{2}(v_{2k_x,2k_y}^j - v_{2k_x,2k_y+1}^j + v_{2k_x+1,2k_y}^j - v_{2k_x+1,2k_y+1}^j) \\
&= < v, \Psi_{k_x}^{j-1}\Phi_{k_y}^{j-1} > \\
v_{k,3}^{j-1} &= \frac{1}{2}(v_{2k_x,2k_y}^j - v_{2k_x,2k_y+1}^j - v_{2k_x+1,2k_y}^j + v_{2k_x+1,2k_y+1}^j) \\
&= < v, \Psi_{k_x}^{j-1}\Psi_{k_y}^{j-1} > \qquad (3)
\end{aligned}$$

where $\Psi(x) = 0.5$ on $[0, \frac{1}{2}[$, -0.5 on $[\frac{1}{2}, 1]$ and zero elsewhere. Consequently, this decomposition satisfies:

$$v_k^j = v_k^{j-1} + v_{k,1}^{j-1} + v_{k,2}^{j-1} + v_{k,3}^{j-1}.$$

The last three quantities in (3) define the horizontal, the vertical and the diagonal details coefficients respectively. This decomposition corresponds to the well known Haar basis (Haar 1910) and defines the simplest orthogonal wavelet decomposition. The main advantage of the Haar basis is that it is orthogonal with minimal support. We justify in the following why small support and orthogonality are important for our purpose.

3 Property of Piecewise Smooth Images with Contours of Non-zero Length

In this section we study the decay of the energy of the coefficients v_k^j,

$$E^j = \sum_{k \in \{0,\cdots,2^j-1\}^2} \left(v_k^j\right)^2,$$

for PSI. We will also need to consider the energy of the detail coefficients:

$$F^j = \sum_{l=1}^{3} \sum_{k \in \{0,\cdots,2^j-1\}^2} \left(v_{k,l}^j\right)^2.$$

The study of the decay of E^j is based on the behavior of the quadratic linear error defined, for the $M = 2^{j'}$ lowest frequencies coefficients, by:

$$\epsilon[M] = \sum_{j=j'+1}^{J-1} F^j.$$

If the image v is PSI then $\epsilon[M]$ decays like $M^{-\frac{1}{2}}$ (Mallat 1998), for large M and in the case of infinite resolution ($J = +\infty$). For such images, the decay of the energy through scales is driven by the decay of the wavelet coefficients in the neighborhood of the edges. If we assume that this decay is valid for PSI with finite resolution, we have the following theorem:

Theorem 1 *For PSI the ratio:*

$$R^j = E^{j-1}/E^j$$

decreases from $j = J$ and does not otherwise.

Proof of Theorem 1: If we keep $M = 2^{2(J-1)}$ coefficients out of $N^2 = 2^{2J}$ and if we put $\epsilon[2^{2(J-1)}] = \alpha = F^{J-1}$, then there exists K such that $\alpha = K/2^{J-1}$ that is $K = \alpha 2^{J-1}$. Computing the value of the function $y = K/\sqrt{x}$ in $x = 2^{2j}$, we have $y = 2^{J-1-j}\alpha$. The quadratic error $\epsilon[2^{2(J-2)}] = 2\alpha$ is also equal to $F^{J-2} + F^{J-1}$ which leads to $F^{J-1} = F^{J-2}$. Continuing, when $x = 2^{2(J-3)}$, $y = 4\alpha$ which implies $F^{J-3} = 2F^{J-2}$. If we now use the orthogonality of the decomposition, i.e.

$$E^j = E^{j-1} + F^{j-1}$$

we get $R^j = 1 - F^{j-1}/E^j$. Since F^{j-1} increases and E^j decreases when j decreases, R^j decreases when j decreases.

For images that are non-PSI, $\epsilon[M]$ typically decays more slowly than $M^{-\frac{1}{2}}$ at small scales (i.e. large j). This implies that F^j decreases at least between scales $J-1$ and $J-2$, using the same reasoning as previously. As E^j also decreases when j decreases we have to study their respective decay. Since $0 \geq F^{J-2} - F^{J-1} \geq -F^{J-1}$ and $E^{J-1} - E^J = -F^{J-1}$, F^{j-1} decays more slowly than F^j between scales J and $J-1$, which implies that R^j increases between scales J and $J-1$ $\blacksquare$.

We illustrate Theorem 1 on the images of Figure 1 which are either extracted from the Brodatz album (Brodatz 1966) or from VisTex database (VisTex 1995). To study the robustness of the criterion to a variation of the block size, we split each texture patches into non-overlapping blocks and we compute the first two ratios R^J and R^{J-1}. The percentage of blocks that can be viewed as PSI is given in Table 1 as a function of the block size. The criterion used is thus efficient to distinguish oscillatory structures from more regular ones. In applications, the smallest blocks as possible are required to avoid the mixing of regions of different kind: the only appropriate sizes to compute our criterion are blocks of size 32×32 or 16×16. Note that the block size must be a power of 2 due to the downsampling generated by the orthogonal wavelet decomposition.

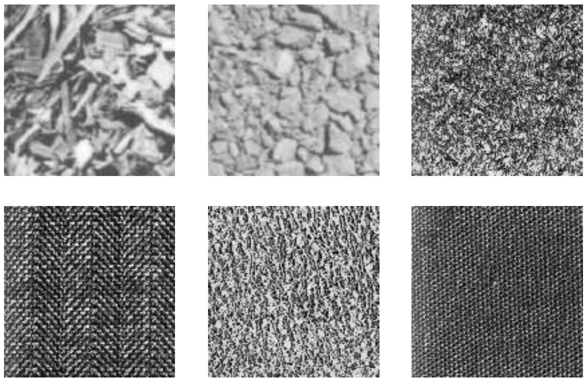

Fig. 1. Brodatz images used to test the criterion; from left to right and top to bottom VisTex Textures "Misc and rock" and Brodatz textures "D9,D17,D24,D77"

4 Noise Variance Estimation

In this section, we propose a new algorithm to compute the noise variance for white noise and also for $1/f$ noise since many sensors introduce a noise that can be spectrally correlated. We first explain how the decay of the ratio R^j for a region that is PSI enables to retrieve it in a noisy context. We then use this study to identify the subregions of a noisy image that are PSI. Finally, we estimate the noise variance on the identified subregions for the two families of noises.

	Misc	Rock	D9	D17	D24	D77
block size $= 128 \times 128$	100	100	0	0	0	0
block size $= 64 \times 64$	100	100	0	0	0	0
block size $= 32 \times 32$	100	100	0	6	0	0
block size $= 16 \times 16$	100	100	0	12	0	0
block size $= 8 \times 8$	94	93	5	26	5	1

Table 1

Computation of the percentage of PSI blocks for varying block size for the images of Figure 1

We consider the following model for noisy images:

$$\tilde{v}_k^J = v_k^J + d_k^J \tag{4}$$

where v is the original signal and d is a two dimensional noise with standard deviation σ_a. The model for images (4) leads to the relations:

$$\tilde{v}_{k,i}^j = v_{k,i}^j + d_{k,i}^j \qquad \tilde{v}_k^j = v_k^j + d_k^j \tag{5}$$

Due to the orthogonality of the Haar basis and due to the independence of the noise from the signal, we can write for $j \leq J$:

$$\tilde{E}^j = E^j + E_d^j, \tag{6}$$

where $\tilde{E}^j$ (resp E_d^j) is the energy of $\tilde{v}_k^j$ (resp. d_k^j).

4.1 PSI retrieval and White Noise

In this section, we assume that the noise is white. Donoho and Johnstone (Donoho and Johnstone 1994) showed that for PSI the number of large detail coefficients that correspond to edges at scale $J-1$ is small (i.e. $v_{k,i}^{J-1}$ is negligeable compared with d_k^{J-1} in (5)) which enables white noise standard deviation estimation with the normalized median of the absolute value of the coefficients $\tilde{v}_{k,i}^{J-1}$, $i = 1, \cdots, 3$, i.e. $\hat{\sigma}_a = median((|\tilde{v}_{k,i}^{J-1}|_{k,i=1,\cdots,3}))/0.6745$. This technique is referred to as Donoho's method in the following.

Since a white noise decomposed over an orthonormal basis is still white with the same variance (Mallat 1998), the wavelet coefficients $d_{k,i}^j$ are of zero mean with variance σ_a^2. This implies that $E_d^j = N^2/4^{J-j} \times \sigma_a^2$, taking into account the downsampling factor that arises from orthogonal dyadic decomposition. We then use the following observation: the estimated noise variance $\hat{\sigma}_a^2$ on a PSI is close to the true noise variance σ_a^2. On these regions we can, consequently, compute a good estimation of E^j through:

$$E^j \approx \hat{E}^j = \tilde{E}^j - N^2/4^{J-j} \times \hat{\sigma}_a^2$$

Because of the good approximation of the noise variance, the ratio $\hat{R}^j = \hat{E}^{j-1}/\hat{E}^j$ is decreasing on the images that are PSI. On non-PSI images, $\hat{R}^j$ can exhibit very different behaviors. The only thing we know is that the number of coefficients that do not correspond to noise at small scales (i.e. $J-1$) are more numerous than for PSI which leads to an important overestimation of the noise variance. This overestimation has a greater impact on small scales (large j) since:

$$\hat{E}^j - E^j = N^2/4^{J-j} \times (\sigma_a^2 - \hat{\sigma}_a^2).$$

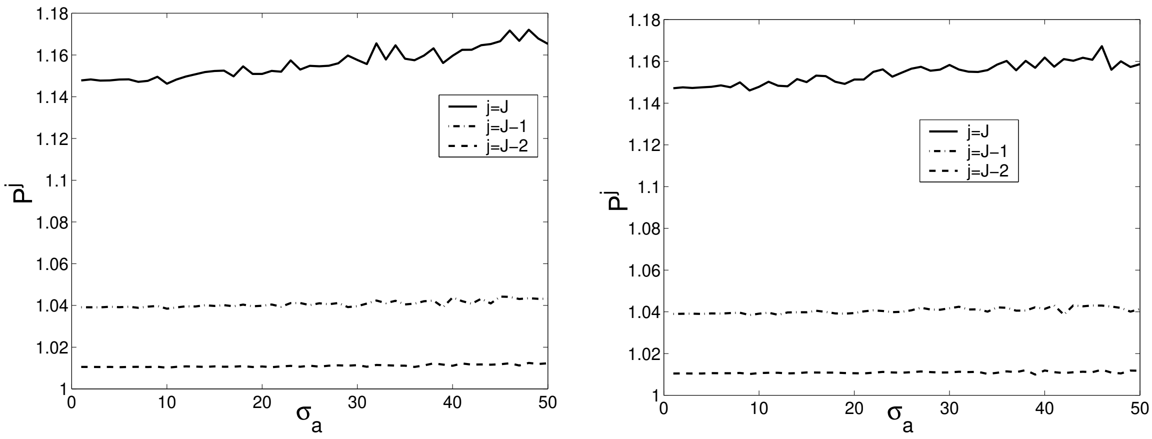

(A) (B)

Fig. 2. Computation of the ratio $P^j = \hat{R}^j / R^j$ averaged over the last four images of Figure 1, with respect to the standard deviations of a uniform white noise (A) and of a Gaussian white noise (B) for $j = J, J-1, J-2$

This means that E^j is underestimated by $\hat{E}^j$ for large j which leads to $\hat{R}^j$ larger than R^j. Indeed, this means that:

$$\left(E^{j-1} + \frac{N^2}{4^{J-j+1}}(\sigma_a^2 - \hat{\sigma}_a^2)\right) / \left(E^j + \frac{N^2}{4^{J-j}}(\sigma_a^2 - \hat{\sigma}_a^2)\right) \geq E^{j-1}/E^j \Leftrightarrow R^j \geq 1/4,$$

which is always satisfied for the images under consideration. Furthermore, we numerically notice that we have a very fast convergence of the estimated ratio $\hat{R}^j$ to the ratio R^j when j decreases. Indeed, in Figure 2, we compute the ratio $P^j = \hat{R}^j / R^j$ averaged over the last four images of Figure 1 (which are all non-PSI) for both Gaussian and uniform white noise. We also note that, in both cases, the convergence is relatively independent from the noise level. This convergence entails that when the images are non-PSI the ratio $\hat{R}^j$ is an increasing function for intermediate value of j. The criterion we use to retrieve PSI images is thus the following:

$$\hat{R}^{J-1} < \hat{R}^J, \quad \hat{R}^{J-2} < \hat{R}^{J-1}. \tag{7}$$

To show the relevance of our approach to retrieve PSI, we display, in Figure 3, the percentage of blocks that change classes when the noise level varies. The simulations are carried out both for Gaussian and uniform white noises. We compute the percentage for blocks of size 32×32 extracted either from the first two images of Figure 1 which are all PSI or from the last four images of Figure 1 which are mostly non-PSI. To obtain smoother results we authorize the blocks to overlap. We either use the decay of $\hat{R}^j$ between scales J and $J-1$ as a criterion to compute the class changes (criterion 2 in Figure 3) or the criterion defined by (7) (criterion 1 in Figure 3). We notice in Figure 3 (B) that $\hat{R}^J < \hat{R}^{J-1}$ cannot be used to characterize non-PSI blocks in a noisy context since there is more than 90 % class changes with this criterion regardless of the noise level. On the contrary, the criterion defined by (7) enables to keep most of the non-PSI blocks in their class in the presence of noise. The effect of the criterion (7) on PSI blocks is on the contrary quite

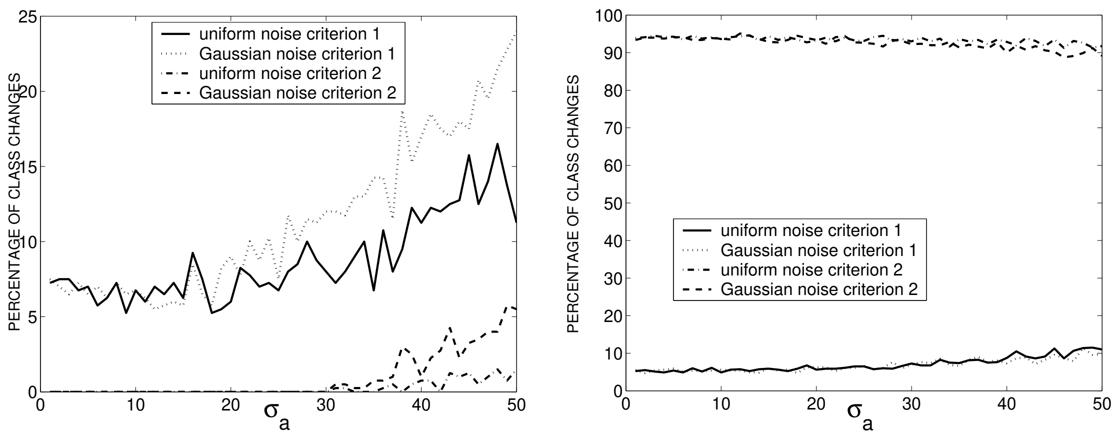

(A) (B)

Fig. 3. (A): Computation of the percentage of class changes, for blocks of size 32×32 pixels extracted from the first two images of Figure 1, using either $\hat{R}^J > \hat{R}^{J-1}$ and $\hat{R}^{J-1} > \hat{R}^{J-2}$ (criterion 1) or $\hat{R}^J > \hat{R}^{J-1}$ (criterion 2); (B): idem but for the blocks extracted from the last four images of Figure 1

small since the percentage of class changes remains inferior to 10 % for the PSI blocks and for a reasonable noise level (see Figure 3 (A)). When we use the decay of $\hat{R}^j$ between scale J and $J-1$ we obtain better results on PSI than with the criterion defined by (7). Nevertheless, the important fact is to define a criterion that keeps most of non-PSI blocks in their class when the noise level increases because those are responsible for bad noise variance estimation. Therefore, the criterion defined in (7) is relevant for our purpose. We also note that the behavior of the criterion is very similar for Gaussian and uniform white noises for a reasonable noise level.

When we consider blocks of size 16×16 pixels, the evaluation of our criterion on PSI blocks becomes much more unstable. The reason is that for such a block size, $\hat{E}^{J-3}$, used in $\hat{R}^{J-2}$, is computed with only 4 coefficients. Therefore, the appropriate size for our simulations will be 32×32 pixels block.

4.2 PSI Retrieval and $1/f$ noise

In this section, we assume that the noise is such that its Fourier spectra behaves like $1/f^{\gamma}$. There are many physical phenonema for which the value of γ lies in the range $]0, 2[$ (Keshner 1982). With this condition put on γ, Wornell (Wornell 1990) proved that the one dimensional limit process:

$$x(t) = \lim_{M \to -\infty} \sum_{j \geq M} \sum_{k \in \mathbb{Z}} \alpha_k^j \Psi_k^j(t),$$

where $(\Psi_k^j)_{(k,j) \in \mathbb{Z}^2}$ is an orthogonal wavelet basis of $L^2(\mathbb{R})$ (the space of square integrable functions), is such that its Fourier spectra behaves like $1/f^{\gamma}$ when the following conditions are fulfilled:

- α_k^j and $\alpha_k^{j'}$ are uncorrelated

- α_k^j and $\alpha_{k'}^j$ are uncorrelated
- The variance of $(\alpha_k^j)_k$ is of the form $\sigma_b^2 2^{-\gamma j}$
- The function Φ is such that the modulus of its Fourier transform $|\hat{\Phi}(f))| \leq C/(1+|f|)$

The demonstration of Wornell (Wornell 1990) is still valid when one switches from one dimension to two dimensions. Indeed, define $\Psi_{k,1}^j = \Phi_{k_x}^j \Psi_{k_y}^j$, $\Psi_{k,2}^j = \Psi_{k_x}^j \Phi_{k_y}^j$ and $\Psi_{k,3}^j = \Psi_{k_x}^j \Psi_{k_y}^j$, such that $(\Psi_{k,1}^j, \Psi_{k,2}^j, \Psi_{k,3}^j)_{k\in\mathbb{Z}^2, j\in\mathbb{Z}}$ is an orthogonal basis of $L^2(\mathbb{R}^2)$. Then, the limit process:

$$I(x,y) = \lim_{M\to-\infty} \sum_{k\in\mathbb{Z}^2} \sum_{i=1}^{3} \sum_{j\geq M} d_{k,i}^j \Psi_{k,i}^j(x,y)$$

is such that its Fourier spectra behaves like $1/f^\gamma$ when the following conditions are fulfilled:

- $d_{k,i}^j$ and $d_{k,i'}^{j'}$ are uncorrelated for all $(i',j') \neq (i,j)$
- $d_{k,i}^j$ and $d_{k',i}^j$ are uncorrelated
- The variance of $(d_{k,i}^j)_k$ is of the form $\sigma_b^2 2^{-\gamma j}$
- The function $g(x,y) = \Phi(x)\Phi(y)$ is such that its two dimensional Fourier transform satisfies $|\hat{g}(f)| \leq C'/(1+\|f\|)$.

Note that with our choice for Φ this last condition is fulfilled.

In image processing, the finite resolution imposes $0 \leq j \leq J$ and that k evolves on a finite lattice. However, we can still have processes very close to $1/f^\gamma$ processes considering Gaussian coefficients $(d_{k,i}^j)_k$ with variance $\sigma_b^2 2^{-\gamma j}$. We propose to estimate σ_b when the parameter γ is known using the characterization of PSI.

An estimation of the standard deviation of the coefficients $\left(d_{k,i}^{J-1}\right)_{k,i=1,\cdots,3}$ can be accurately computed at scale $J-1$ on PSI images with Donoho's method (see the beginning of section 4) since at scale $J-1$ the noise coefficients are a white noise. This estimation denoted by $\hat{\sigma}_{1/f}$ does not correspond to the standard deviation of the noise in the image but approximates $\sigma_b 2^{-\gamma(J-1)/2} = \sigma_{1/f}$. We can, therefore, write the following approximation $\sigma_b \approx \hat{\sigma}_{1/f} \times 2^{\gamma(J-1)/2}$ and then deduce that on PSI:

$$E^j = \tilde{E}^j - N^2/4^{J-j} \times \sigma_b^2 2^{-\gamma j} \approx \hat{E}^j = \tilde{E}^j - N^2/4^{J-j} \times \hat{\sigma}_{1/f}^2 2^{\gamma(J-j-1)}$$

For non-PSI images, $\hat{\sigma}_{1/f}$ is an overestimation of the true standard deviation of the coefficients $(d_{k,i}^{J-1})_{k,i=1,\cdots,3}$. Since:

$$\hat{E}^j - E^j = N^2/(2^{(2-\gamma)(J-j)-\gamma}) \times (\sigma_{1/f}^2 - \hat{\sigma}_{1/f}^2),$$

for $\gamma \in]0,2[$, $\hat{E}^j$ tends to E^j when j decreases and $\hat{R}^j \geq R^j$ provided $R^j \geq \frac{1}{2^{2-\gamma}}$ making the same computation as for white noises (see previous section).

We now study the evolution of $\hat{R}^j$ with respect to j and γ for non-PSI images. We display on Figure 4 the typical evolution of $P^j = \hat{R}^j/R^j$ for different values of γ when the coefficients $(d_{k,i}^j)_k$ are uniform and white with variance $\sigma_b^2 2^{-\gamma j}$. When γ is small, typically $\gamma < 1$ the behavior of $\hat{R}^j$ is very similar to that obtained with a white noise. When γ is larger, the ratio $\hat{R}^j$ is very close to R^j even for large j. Similar results can be obtained when $(d_{k,i}^j)_k$ are Gaussian and white but we do not show them due to the lack of space.

The evolution of $\hat{R}^j$ tells us what criterion to use: when γ is small one had better use the criterion (7) due to the relatively bad estimation $\hat{R}^j$ of R^j and, for larger γ, the criterion $\hat{R}^J > \hat{R}^j$ should be sufficient. We now check this hypothesis, still when $(d_{k,i}^j)_k$ are uniform and white (similar results are

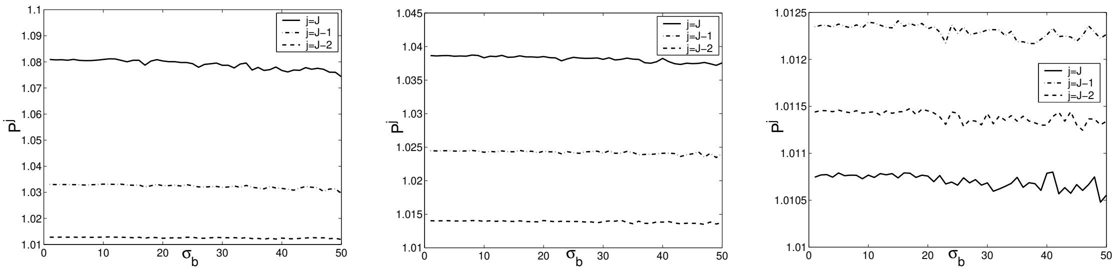

(A) (B) (C)

Fig. 4. (A): evolution of the ratio P^j averaged over the last four images of Figure 1 for $\gamma = 0.5$, (B): idem but for $\gamma = 1$,(C): same computation but for $\gamma = 1.5$

obtained when these coefficients are Gaussian and white).

We compute the percentage of class changes for blocks of size 32×32 extracted either from the first two images of Figure 1 (see Figure 5 (A)) or from the last four images of Figure 1 (see Figure 5 (B)), when σ_b varies and γ equals 0.5 or 1. We notice that, when $\gamma = 0.5$, the criterion (7) (denoted by criterion 1 in Figure 5) keeps all the non-PSI images in their class as well as most of the PSI images in their class (the percentage of class changes is about 10 % for a reasonable noise level). As we are interested in keeping the non-PSI images in their class, the criterion (7) is better than $\hat{R}^J > \hat{R}^{J-1}$ (criterion 2 in Figure 5) for small values of γ . On the contrary when $\gamma = 1$, the number of class changes for non-PSI images are similar with the two criteria (see Figure 5 (B)) but the number of class changes for PSI is larger for PSI images with the criterion (7) than with the other. We also checked that this conclusion holds for $\gamma > 1$. This allows us to conclude that to discriminate PSI blocks from non-PSI blocks, one had better use the criterion (7) when γ is small and, $\hat{R}^J > \hat{R}^{J-1}$ for larger γ.

A last point to mention is that with the criterion (7) we have to consider blocks of size at least equal to 32×32 pixels which is no longer the case with the criterion $\hat{R}^J > \hat{R}^{J-1}$. Therefore, we also compute the percentage of class changes with a block size 16×16 when $\gamma = 1$. In this case, we notice very little differences with the results obtained with the block size 32×32 pixels.

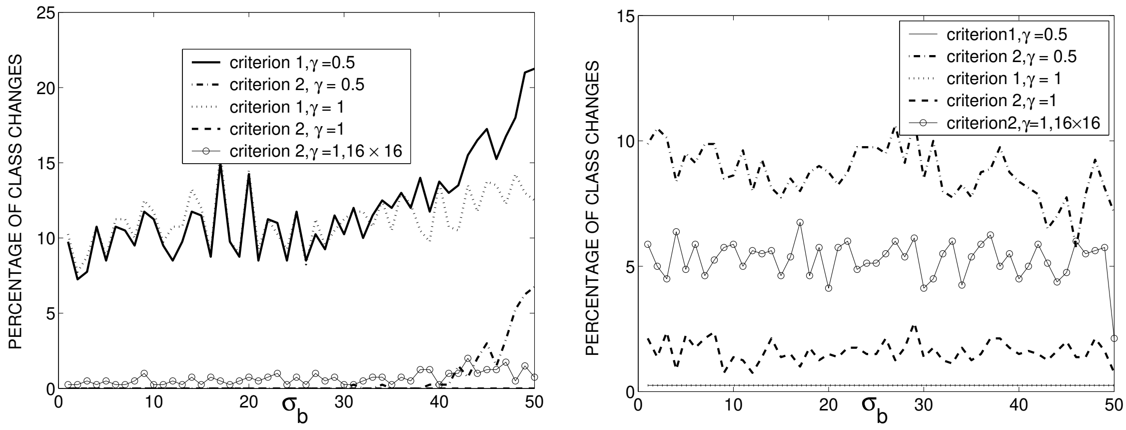

(A) (B)

Fig. 5. (A): Computation of the percentage of class changes, for blocks extracted from the first two images of Figure 1, using either $\hat{R}^J > \hat{R}^{J-1}$ and $\hat{R}^{J-1} > \hat{R}^{J-2}$ (criterion 1) or $\hat{R}^J > \hat{R}^{J-1}$ (criterion 2), with $\gamma = 0.5$ or 1. The block size is 32×32 pixels except for the last case (criterion 2 , $\gamma = 1$), where we also consider the block size 16×16 pixels; (B): idem but for the blocks extracted from the last four images of Figure 1.

5 Algorithm for Noise Variance Computation

Referring to the previous study, the principle of the algorithm for the retrieval of PSI subregions of a noisy image is to split the original image into small subregions of equal size and to compute the estimation of the standard deviation of the noise or the estimation of σ_b on each subregion. The procedure is summarized as follows:

- Split the original image into subimages of equal size.
- Perform a orthonormal wavelet decomposition of each subimage.
- Compute the standard deviation of the noise or the estimation of σ_b (depending on the case) with Donoho's method on each subimage
- Remove the non-PSI regions.
- Compute the estimation of the standard deviation of the noise or the estimation of σ_b using the coefficients associated with the remaining subimage.

In the following, we call local estimators those obtained with such an algorithm. We must stress here that as we perform wavelet decompositions on small domains, the support of the wavelet has to be the smallest as possible to avoid boundary artifacts. Therefore, decomposition of the image on the Haar wavelet basis is appropriate.

6 Results

An artificial example

We first give an illustration of the subimage selection procedure for image (A) of Figure 6 which is a mixture of the VisteX database (VisTex 1995) image "rock" and of the Brodatz texture "D77" when there is no additive noise. We surround in white the regions that are estimated as non-PSI.

Then, for PSI regions determination and for white noise variance estimation, the size of the blocks we use is 32×32. We only consider a uniform white noise but similar conclusions can be derived for a Gaussian white noise. In Figure 6

(B), we display the results of local noise variance estimation procedure compared to a global estimation made on the whole image (Donoho and Johnstone 1994). We note that the local estimator of the noise we propose is not biased while the global one is.

For $1/f$ noises we consider $\gamma = 0.5$ and $\gamma = 1$ in which cases the wavelet coefficients $(d^j_{k,i})_{k,i=1,\cdots,3}$ are uniformly distributed and white. We focus on the estimation $\hat{\sigma}_b$ of σ_b. In the first case ($\gamma = 0.5$), we consider a block size of 32×32 pixels and the criterion (7) to retrieve PSI. In the second case ($\gamma = 1$), we either use blocks of size 32×32 pixels or 16×16 pixels and the criterion $\hat{R}^J > \hat{R}^{J-1}$ to retrieve PSI regions. In Figure 6 (C)-(D), we display the estimation $\hat{\sigma}_b$ of σ_b. We notice that in these cases also our estimator behaves much better than the global one and that the local estimator is all the better that γ is large. To take blocks of size 32×32 pixels or 16×16 pixels makes no difference when $\gamma = 1$, for this image.

A Natural Image Example

We give another illustrative example of the behavior of the noise standard deviation estimator and of the estimation of σ_b for the image of Mandrill (see Figure 7 (A)).

In Figure 7 (B), we compute the estimation of the standard deviation of a uniform white noise using both global and local estimators. The size of the subimages for PSI local noise variance estimation is still 32×32 pixels. We notice that the local standard deviation estimation outperforms the global estimator (similar results could be obtained with a Gaussian white noise). We also not that contrary to the case studied before, the difference between the two kinds of estimators diminishes when the noise level increases.

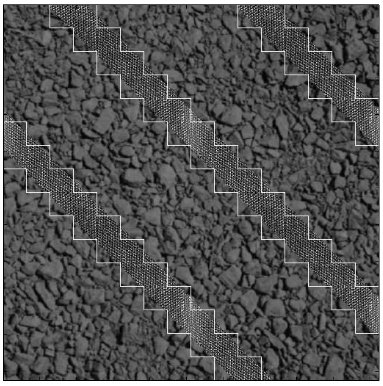

(A)

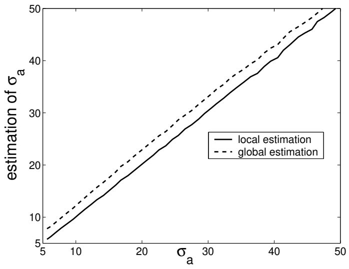

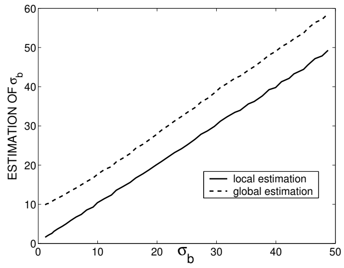

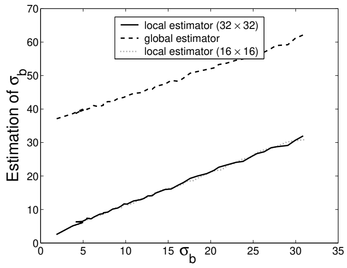

(B) (C) (D)

Fig. 6. (A): Original image with the non-PSI regions surrounded in white. (B): Global and local estimators of the noise standard deviation as a function of the theoretic standard deviation for uniform white noise. (C): Global and local estimators of σ_b for $1/f$ noises and $\gamma = 0.5$, the block size being 32×32 pixels. (D): idem but for $\gamma = 1$ the block size for the estimation of σ_b being either 32×32 or 16×16.

As far as the $1/f$ noise is concerned, we compute the estimator of σ_b on PSI regions where the size of the region is 32×32 pixels for $\gamma = 0.5$ and we note that the local estimator we propose outperforms the global one. When $\gamma = 1$ and with a block size 32×32 pixels, the local estimator of σ_b on PSI provides a underestimation of σ_b. For low noise level, we can however still say that this estimator is better than the global one. We do not display the results of our simulations with blocks of size 16×16 pixels since the results are similar than with the blocks of size 32×32 pixels that is to say not very satisfactory.

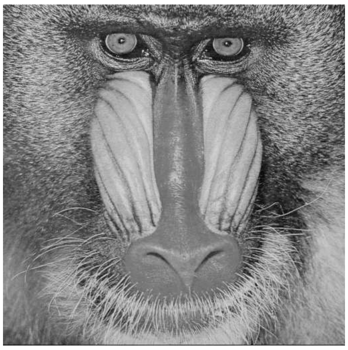

(A)

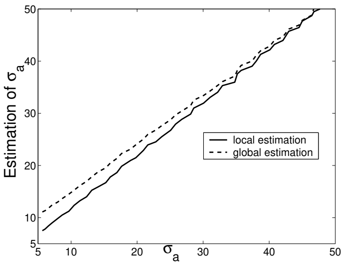

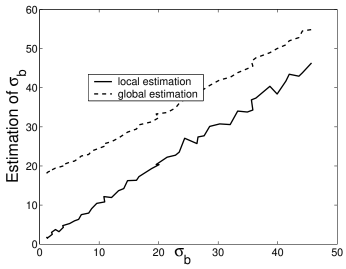

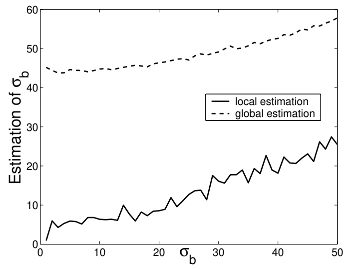

(B) (C) (D)

Fig. 7. (A): Image of Mandrill,(B): uniform white noise standard deviation estimation with global (dashed line) and local estimator (solid line). (C): estimation of σ_b in the uniform case, for $\gamma = 0.5$ and a block size 32×32.(D): same as (C) but $\gamma = 1$

7 Conclusion

The aim of this paper was to adapt the algorithm initially proposed by Donoho for noise variance estimation to the case of images made of homogeneous regions with contours of non-zero length (denoted PSI here) and of more oscillatory regions. We showed that the study of the decay of the energy through scales provides an interesting tool for characterizing the first kind of regions. We then explained how to use this characterization in a noisy context to remove oscillatory structures from the image before noise variance estimation or before the estimation of σ_b for $1/f$ noise. To proceed this way is interesting, since these structures are responsible for the bad estimations.

In a wavelet framework, white and $1/f$ noises have simple characterizations which enabled us to derive algorithms for their respective parameters estimation. However, in spite of the good performances of the estimator we propose, we must note that for large γ, for $1/f$ noise, there is still some work to do to reach a good approximation of σ_b in natural scene. Another direction for future work is the joint estimation of γ and σ_b in natural images.

References

[Brodatz 1966] Brodatz P., 1966. Textures : A Photographic Album for Artists and Designers, Dover, New York.

[Donoho and Johnstone 1994] Donoho D. and Johnstone I., 1994. Ideal Spatial Adaptation Via Wavelet Shrinkage, Biometrika 81, 425-455.

[Haar 1910] Haar A., 1910. Zur Theorie der orthogonalen funktionensysteme, Math. Annal. 69, 331-371.

[Keshner 1982] Keshner M. S., 1982. 1/f noise, Proceedings IEEE 70, 212-218.

[Mallat 1998] Mallat S., 1998. A Wavelet Tour of Signal Processing, Academic Press.

[Rank et al. 1999] Rank K., Lendl M. and Unbehauen R., 1999. Estimation of image noise variance, IEE Proc.-Vis Image Signal Process. 146, 80-84.

[VisTex 1995] VisTex, 1995. Color Image Database, http://www-white.media.mit.edu/vismod/imagery/VisionTexture, MIMedia Lab.

[Wornell 1990] Wornell G. W., 1990. A Karhunen-Loeve-like expansion for $\frac{1}{f}$ processes via wavelets, IEEE Transactions on Information Theory 36, 859-861.